In-situ formed Fe−N doped metal organic framework@carbon nanotubes/graphene hybrids for a rechargeable Zn−air battery

Wenxiu Yang,[a, b] Yelong Zhang,[c] Xiangjian Liu,[a] Lulu Chen,[a] and Jianbo Jia *,[a]

[a] State Key Laboratory of Electroanalytical Chemistry, Changchun Institute of Applied Chemistry, Chinese Academy of Sciences, Changchun, Jilin 130022, China

[b] University of Chinese Academy of Sciences, Beijing 100049, China

[c] Department of Materials Science & Engineering, & Department of Energy and Resources Engineering, College of Engineering, Peking University, Beijing 100871, China

Email: jbjia@ciac.ac.cn

Experimental Section

Materials: Melamine was bought from the Guangfu Chemical Reagent Company. Nafion (5 wt %) was purchased from Sigma–Aldrich. Carbon-supported Pt catalyst (20 wt %, Pt/C) was bought from Johnson Matthey. Ammonium persulfate ($(NH_4)_2S_2O_8$), iron nitrate ($Fe(NO_3)_2 \cdot 9H_2O$) methanol, ethanol, and N,N-dimethylformamide (DMF) were purchased from Beijing Chemical Reagent Company (Beijing, China). 2-Aminoterephthalate (H_2ATA) was purchased from Alfa Aesar. All chemicals were analytical grade and used as received. All aqueous solutions were prepared with ultrapure water from a Water Purifier System (Sichuan Water Purifier Co. Ltd., China).

Apparatus: X-Ray diffraction data were got with model D8 ADVANCE (BRUKER, Cu Kα radiation, λ =1.5406 Å). Transmission electron microscopy (TEM) images were measured with a JEM-2100F high-resolution transmission electron microscope (JEOL Ltd., Japan). X-ray photoelectron spectroscopy (XPS) was performed using Thermo ESCALAB 250 (Thermo Scientific, USA). Nitrogen sorption isotherms were obtained with an ASAP 2020 Physisorption Analyzer (Micrometrics Instrument Corporation). Electrochemical impedance spectroscopy (EIS) measurements were performed by a Zennium electrochemical workstation (Zahner, Germany). Surface-enhanced Raman scattering (SERS) spectra were measured with a Renishaw 2000 model confocal microscopy Raman spectrometer with a CCD detector and a holographic notch filter (Renishaw Ltd., Gloucestershire, U.K.). X-ray absorption fine structure (XAFS) spectroscopy was carried out at 1W2B end station, Beijing Synchrotron Radiation Facility (BSRF). The Co K-edge

spectra were recorded at room temperature in transmission mode. The electrochemical experiments were employed using a CHI842B electrochemical workstation (CH Instruments, Shanghai). Rotating ring-disk electrode (RRDE) techniques were performed on a Model RRDE-3A Apparatus (ALS, Japan) with CHI842B electrochemical workstation. The electrochemical experiments were performed through a three electrode system with a modified glassy carbon electrode (GCE) as the working electrode, an Ag/AgCl (saturated KCl) electrode as the reference electrode, and counter electrode (platinum foil), respectively. The potential, measured against an Ag/AgCl reference electrode, was converted to the E versus the reversible hydrogen electrode (RHE) according to E(*vs.* RHE) = E(*vs*. Ag/AgCl) + 0.059*pH + 0.197. All the electrochemical measurements were carried out at room temperature.

Synthesis of MIL-53(Fe)

MIL-53(Fe) was prepared as described previously with some modifications.[1] In a typical procedure, 0.50 g H_2ATA was dissolved slowly into 10 mL of DMF solution with stirring. And then 1.12 g $Fe(NO_3)_3 \cdot 9H_2O$ was added into the above mixture and stirred for 2 h at room temperature followed by transfer into a Teflon-lined stainless steel autoclave (50 mL) and heated at 150 °C for 6 h. After being cooled naturally to room temperature, the mixture was centrifuged and further purified with DMF and methanol successively, and then, dried in a vacuum at 60 °C for 24 h.

Synthesis of Fe-N doped metal organic framework@carbon nanotube/graphene (Fe-MOF@CNT-G) catalyst

0.20 g of MIL-53 was dissolved into 4 mL ultrapure water and the mixture with ultrasonic for 20 min, followed by adding 0.20 g of $(NH_4)_2S_2O_8$ into the above mixture and further ultrasonic for 20 min.At last, 0.20 g of melamine (2 mL ultrapure water +2 mL ethanol) was added and further ultrasonic for 2 h. The mixture was naturally cooled to room temperature and frozen overnight. The frozen mixture was dried in oven at 110 °C for 3 h.The remaining product was heated in N_2 at 240 and 900 ^oC for 2 and 1 h, respectively, with a heating rate of 2 ^oC/min.

For simplicity, the resulting samples were named as the $F_xN_yM_z$-T for the addition of x g of Fe-MOF, y g of $(NH_4)_2S_2O_8$ and z g of melamine, as well as the pyrolysis temperature (T °C).

Electrocatalytic activity evaluation.

6.0 mg of $F_xN_yM_z$-T or Pt catalyst (20 wt %, Pt/C) was dissolved in a mixture (2.0 mL) of water, isopropyl alcohol, and 5.0 wt % Nafion with a ratio of 20:1:0.075 (v/v/v) by sonication to get 2.0 mg/mL ink. The GCE was polished carefully with 0.3 μm alumina slurries, followed under sonication in acetone, ethanol, and ultrapure H_2O successively, and then dry. A certain amount of the $F_xN_yM_z$-T suspension was dropped onto the GCE surface with a loading amount of 1000 μg cm^{-2}. The modified GCE were dried under the infrared lamp before use.

The ORR experiments were performed in O_2-saturated 0.10 M KOH. Before experiments, all the modified work electrodes were activated by potential cycling from 1.164 to 0.364 V (*vs.* RHE) in 0.10 M KOH at a scan rate of 50 mV s^{-1}. For RRDE and RDE experiments, the polarization curves were obtained by performing a negative-direction sweep of potential at a rate of 5 mV s^{-1} from 1.164 to 0.364 V (*vs.* RHE) in 0.10 M KOH (from 1.156 to 0.256 V (*vs.* RHE) in 0.10 M $HClO_4$). The ring potential was set at 1.264 V (*vs.* RHE) in 0.10 M KOH (1.156 V (*vs.* RHE) in 0.10 M $HClO_4$), respectively. The OER tests were performed in O_2-saturated 0.10 M KOH at a rate of 5 mV s^{-1} from 0.964 to 1.764 V (*vs* RHE).

Zn−air battery test

For the Zn−air battery test, the air electrode was prepared by uniformly coating the as-prepared catalyst ink onto carbon paper then drying it at 80 °C for 4 h. The mass loading was 1.0 mg cm^{-2}. An Zn plate was used as the anode. Both electrodes were assembled into a Zn−air battery, and 6 M KOH containing 0.20 M Zn acetate ($Zn(CH_3COO)_2$ helps to facilitate the reversible Zn electrochemical reactions) was used as the electrolyte unless otherwise stated.

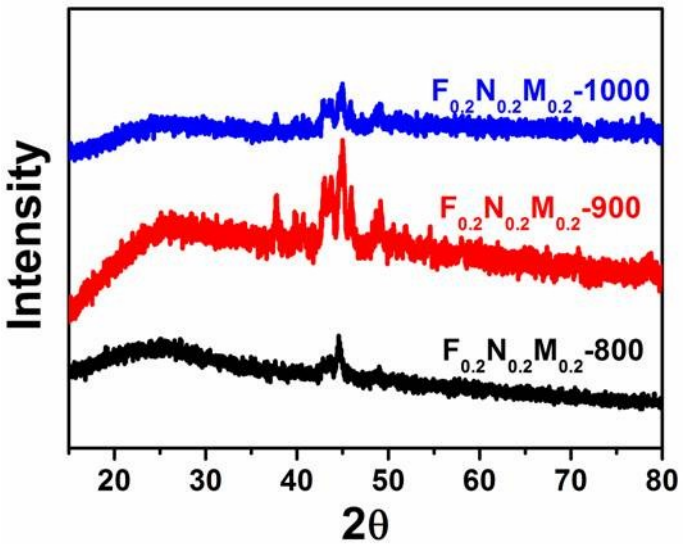

Fig. S1 XRD of $F_{0.2}N_{0.2}M_{0.2}$-800, $F_{0.2}N_{0.2}M_{0.2}$-900, and $F_{0.2}N_{0.2}M_{0.2}$-1000.

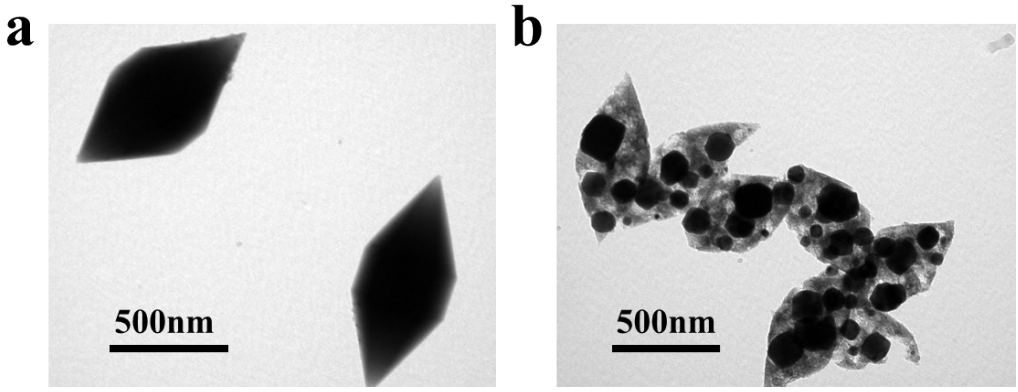

Fig. S2 TEM images of (a) MIL-53(Fe) and (b) MIL-53-900°C.

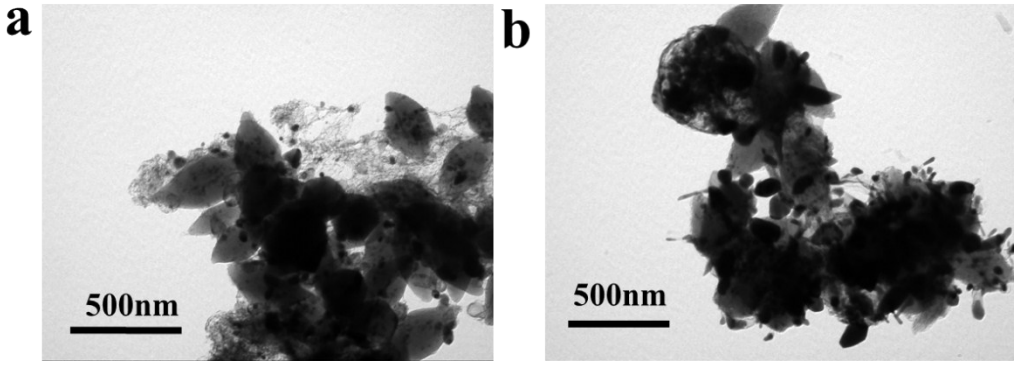

Fig. S3 TEM images of (a) $F_{0.2}N_{0.2}M_{0.2}$-800 and (b) $F_{0.2}N_{0.2}M_{0.2}$-1000.

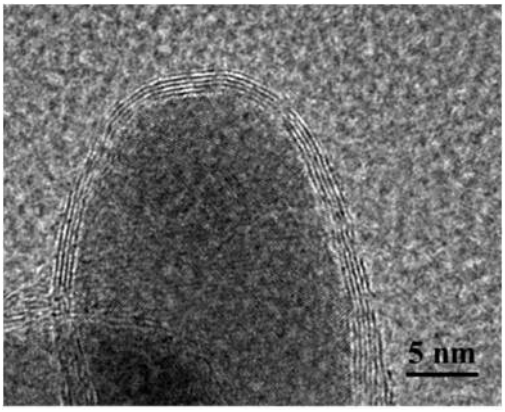

Fig. S4 HRTEM images of the $F_{0.2}N_{0.2}M_{0.2}$-900 material.

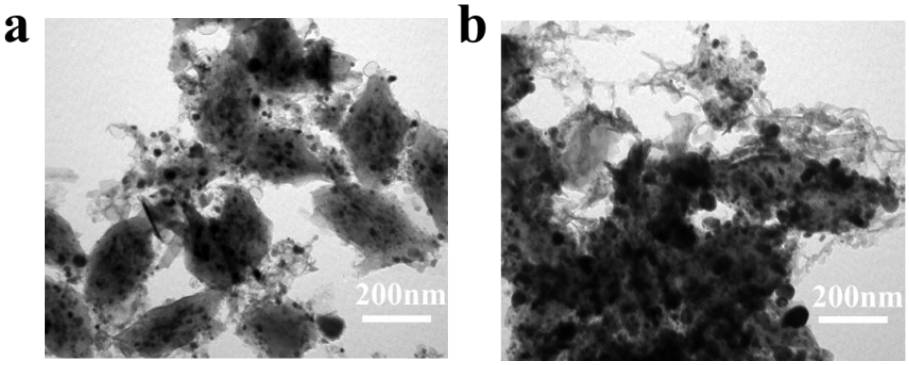

Fig. S5 TEM images of (a) $F_{0.2}N_{0.2}M_0$-900 and (b) $F_{0.2}N_0M_{0.2}$-900.

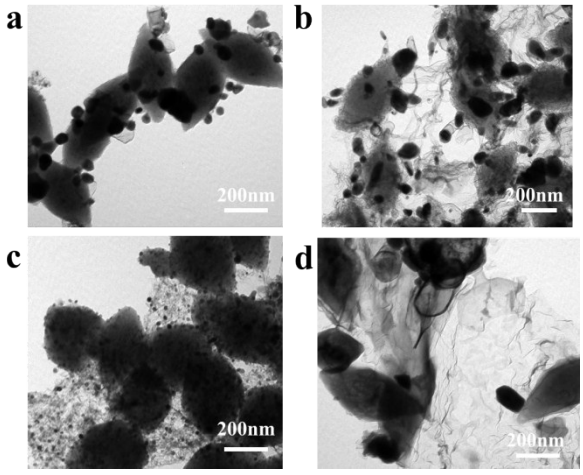

Fig. S6 TEM images of (a) $F_{0.2}N_{0.2}M_{0.1}$-900, (b) $F_{0.2}N_{0.2}M_{0.2}$-900, (c) $F_{0.2}N_{0.2}M_{0.3}$-900, and (d) $F_{0.2}N_{0.2}M_{0.4}$-900.

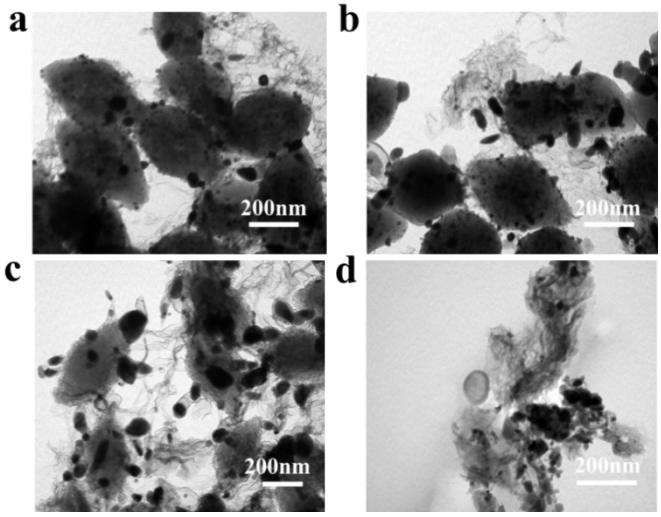

Fig. S7 TEM images of (a) $F_{0.2}N_{0.05}M_{0.2}$-900, (b) $F_{0.2}N_{0.1}M_{0.2}$-900, (c) $F_{0.2}N_{0.2}M_{0.2}$-900, and (d) $F_{0.2}N_{0.3}M_{0.2}$-900.

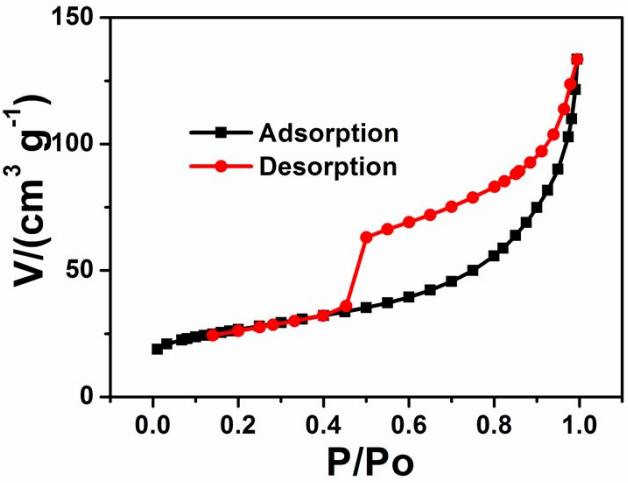

Fig. S8 N_2 adsorption/desorption isotherm of $F_{0.2}N_{0.2}M_{0.2}$-900.

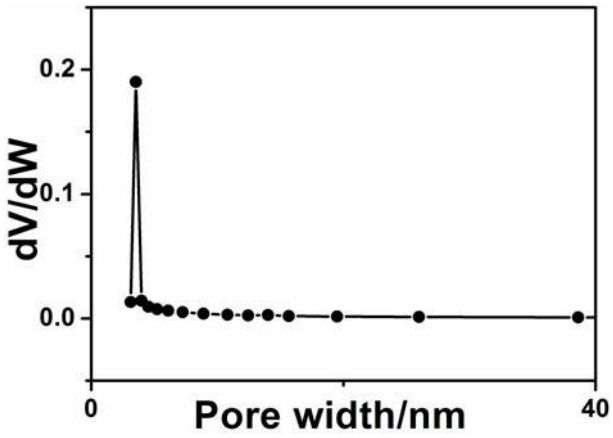

Fig. S9 The pores distribution of the $F_{0.2}N_{0.2}M_{0.2}$-900 material calculated by BJH desorption curves.

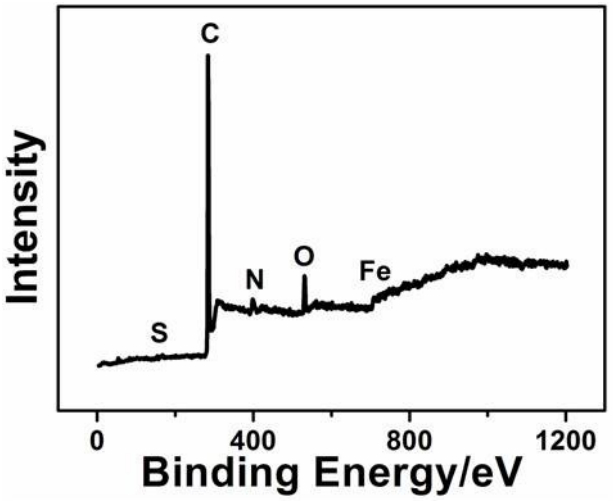

Fig. S10 The XPS of the $F_{0.2}N_{0.2}M_{0.2}$-900 material.

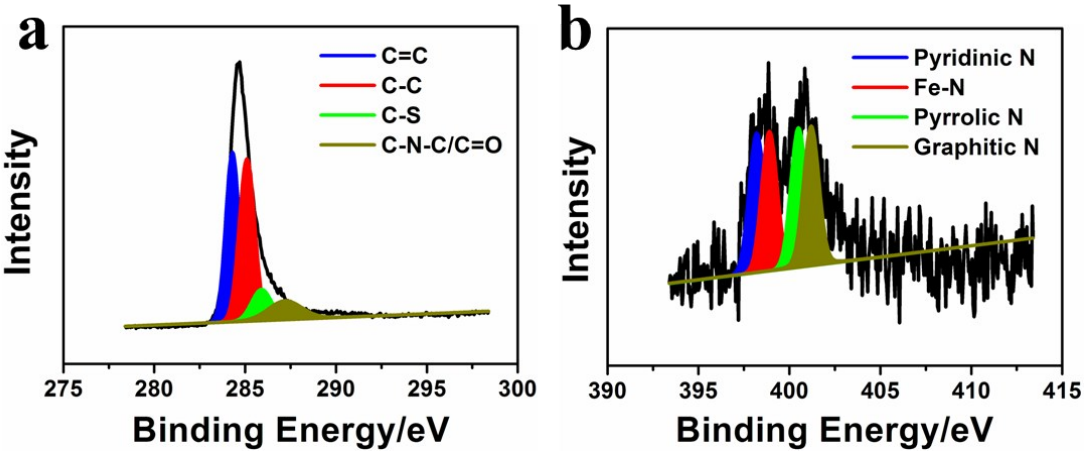

Fig. S11 The high-resolution XPS of the $F_{0.2}N_{0.2}M_{0.2}$-900 material: (a) C1s and (b) N1s.

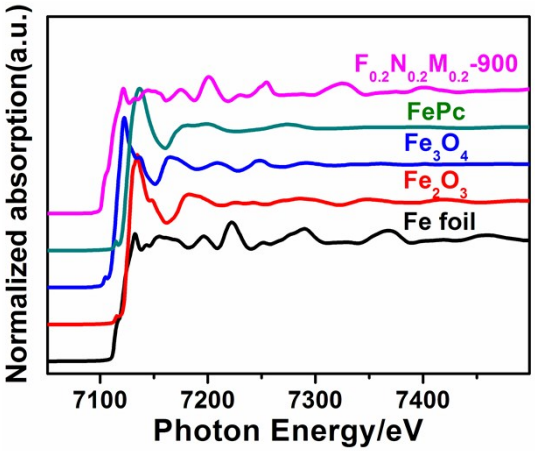

Fig. S12 Fe K edge XANES spectra for different materials.

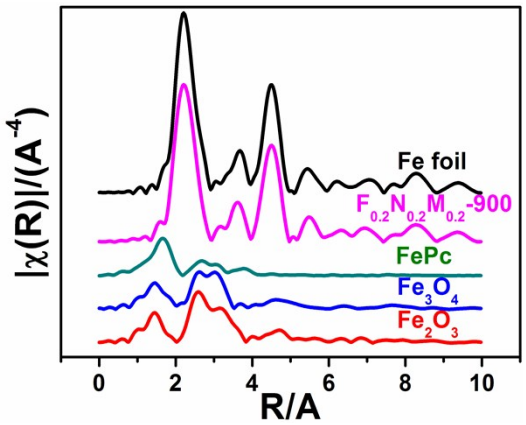

Fig. S13 Fourier transforms of k^3-weighted Fe K-edge EXAFS spectra for different materials.

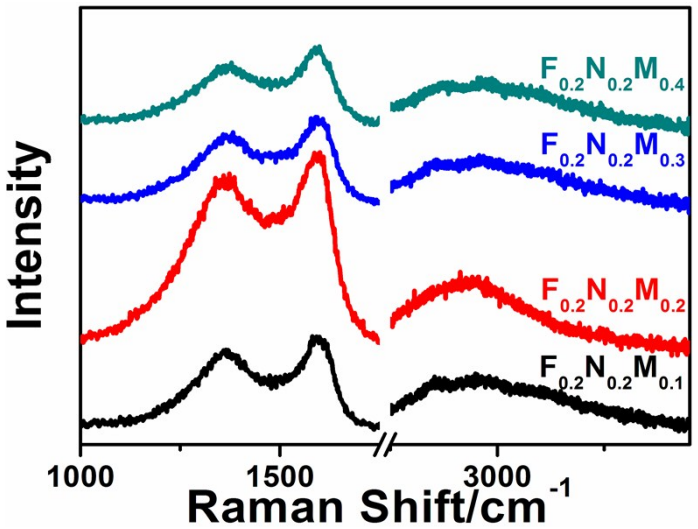

Fig. S14 Raman spectra of different $F_{0.2}N_{0.2}M_z$-*T* samples.

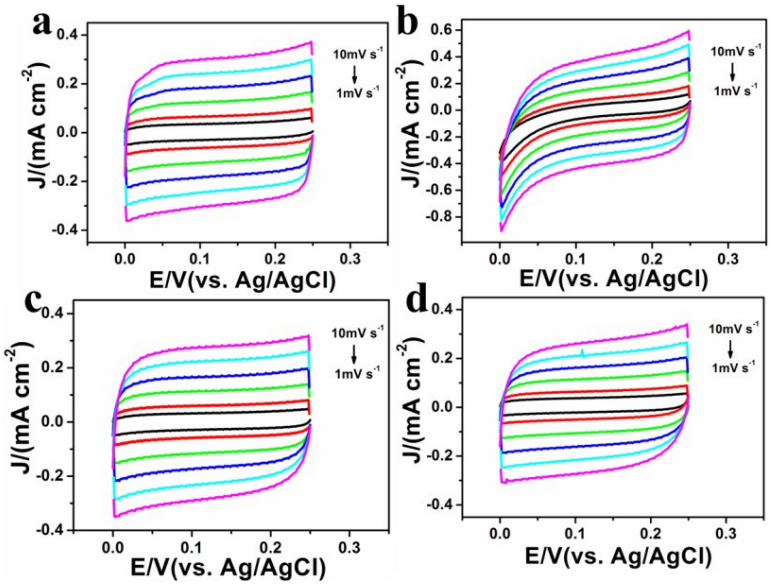

Fig. S15 (a-e) CVs of (a) $F_{0.2}N_{0.2}M_{0.1}$-900, (b) $F_{0.2}N_{0.2}M_{0.2}$-900, (c) $F_{0.2}N_{0.2}M_{0.3}$-900, and (d) $F_{0.2}N_{0.2}M_{0.4}$-900 materials in 0.10 M KOH.

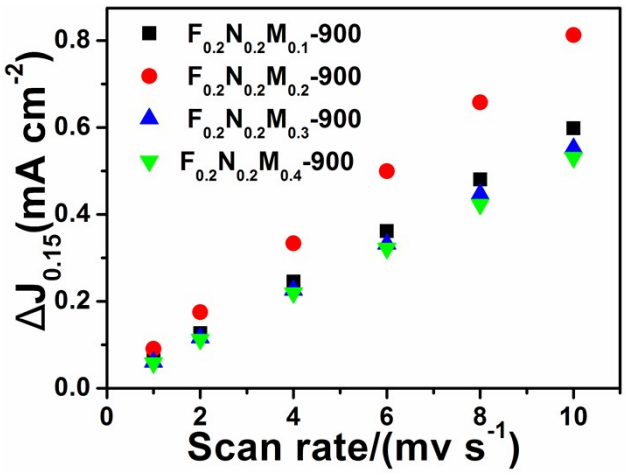

Fig. S16 Plots of ΔJ *vs* scan rate at 0.15 V of different $F_{0.2}N_{0.2}M_z$-*T* samples.

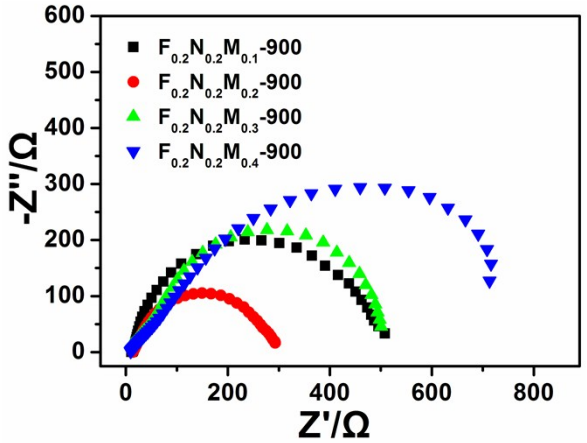

Fig. S17 Nyquist plots of different $F_{0.2}N_{0.2}M_z$-*T* samples.

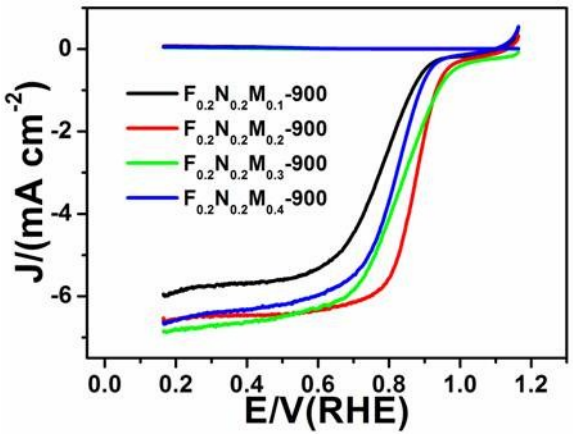

Fig. S18 RRDE voltammograms of different samples in O_2-saturated 0.10 M KOH. The scan rate is 5 mV s^{-1} and the rotation rate is 1600 rpm.

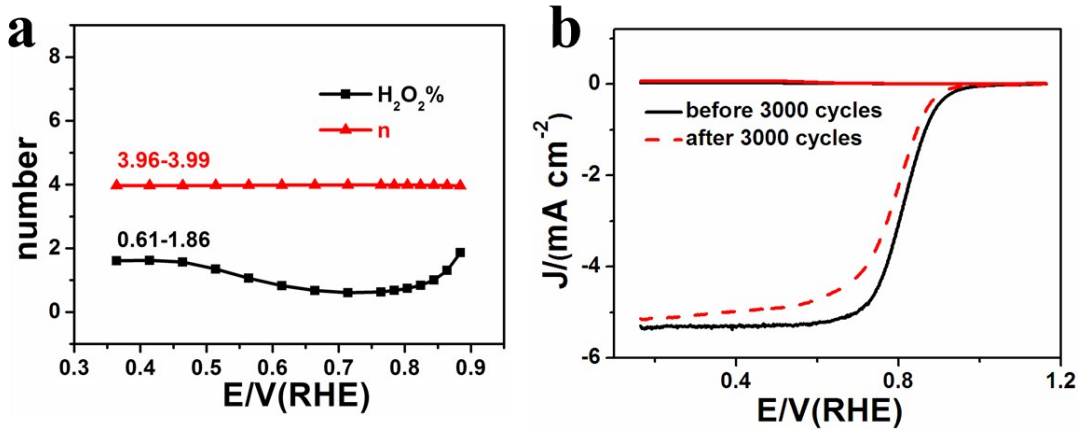

Fig. **S19** (a) H_2O_2% and n of commercial Pt/C in 0.10 M KOH. (b) LSV curves of commercial Pt/C before and after 3000 cycles in 0.10 M KOH. The scan rate is 5 mV s^{-1} and the rotation rate is 1600 rpm.

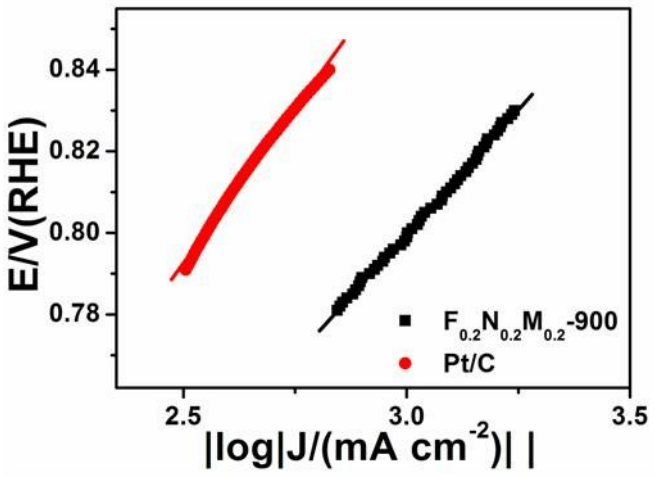

Fig. S20 Tafel plots of the $F_{0.2}N_{0.2}M_{0.2}$-900 and Pt/C electrodes in O_2-saturated 0.10 M $HClO_4$.

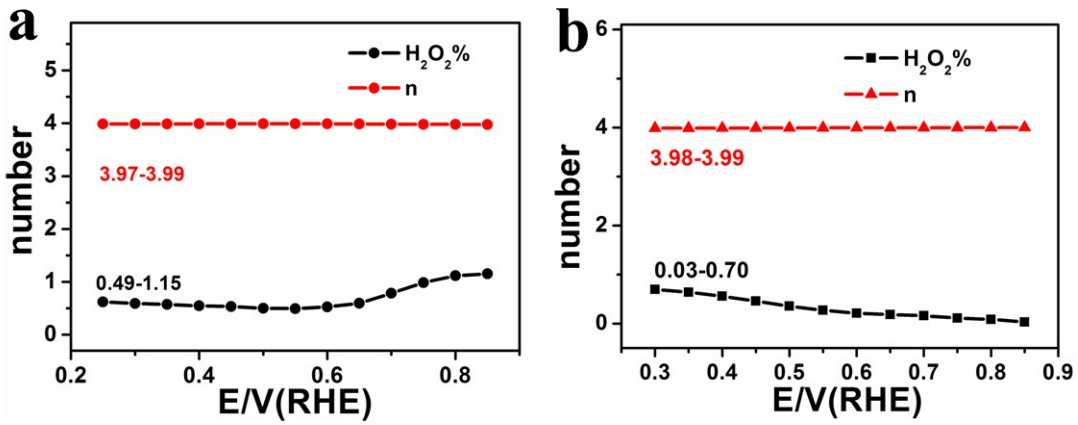

Fig. S21 H_2O_2% and n of the (a) $F_{0.2}N_{0.2}M_{0.2}$-900 and (b) commercial Pt/C catalysts in 0.10 M $HClO_4$.

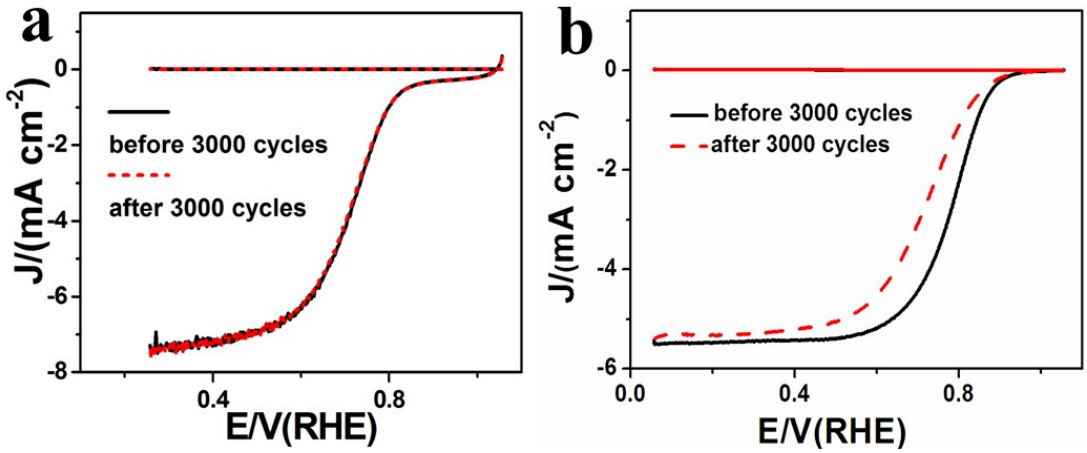

Fig. S22 LSV curves of the (a) $F_{0.2}N_{0.2}M_{0.2}$-900 and (b) commercial Pt/C catalysts before and after 3000 cycles in 0.10 M $HClO_4$. The scan rate is 5 mV s^{-1} and the rotation rate is 1600 rpm.

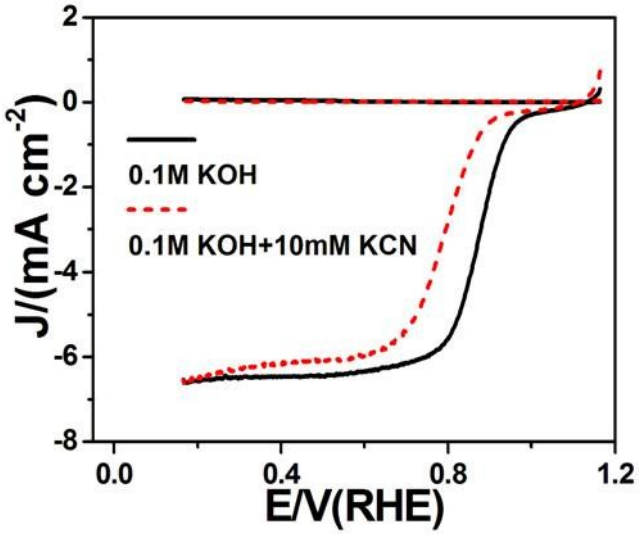

Fig. S23 LSV curves of the $F_{0.2}N_{0.2}M_{0.2}$-900 catalyst with or without the 10 mM KCN in 0.10 M KOH. The scan rate is 5 mV s^{-1} and the rotation rate is 1600 rpm.

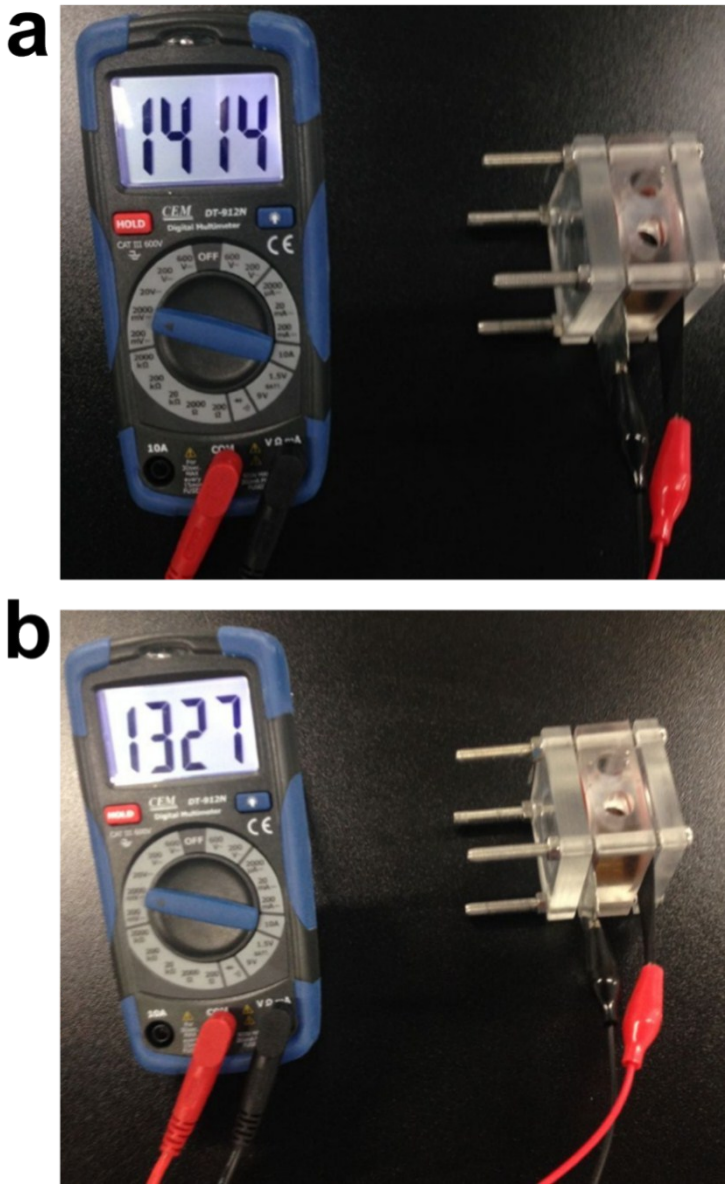

Fig. S24 Photograph of the Zn-air batteries with (a) $F_{0.2}N_{0.2}M_{0.2}$-900 and (b) IrO_2+20% Pt/C catalysts, showing an open–circuit voltage of 1.414 and 1.327 V, respectively.

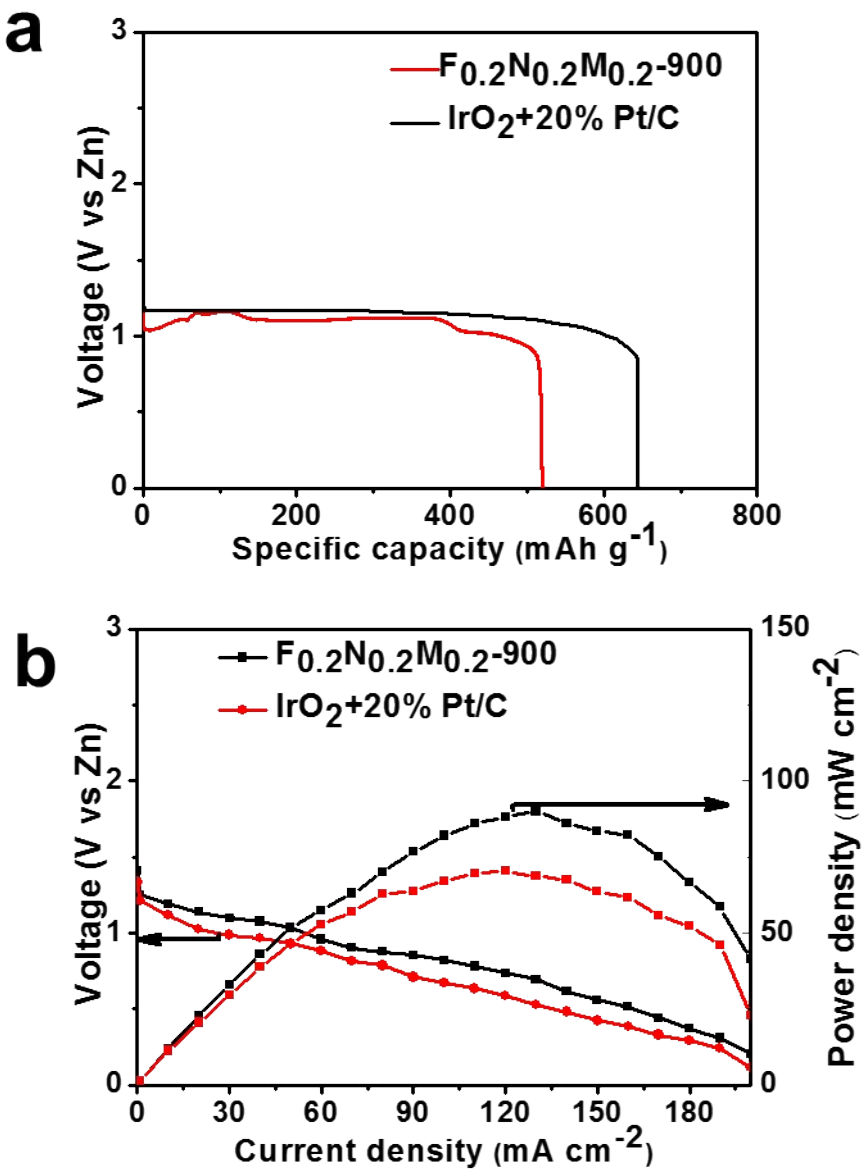

Fig. S25 (a) Typical galvanostatic discharge curves of Zn-air batteries based on $F_{0.2}N_{0.2}M_{0.2}$-900 and IrO_2+20% Pt/C catalysts at a current densities of 10 mA cm^{-2}. The specific capacity was normalized to the mass of consumed Zn anode. (b) Discharge polarization curves and corresponding power density plots.

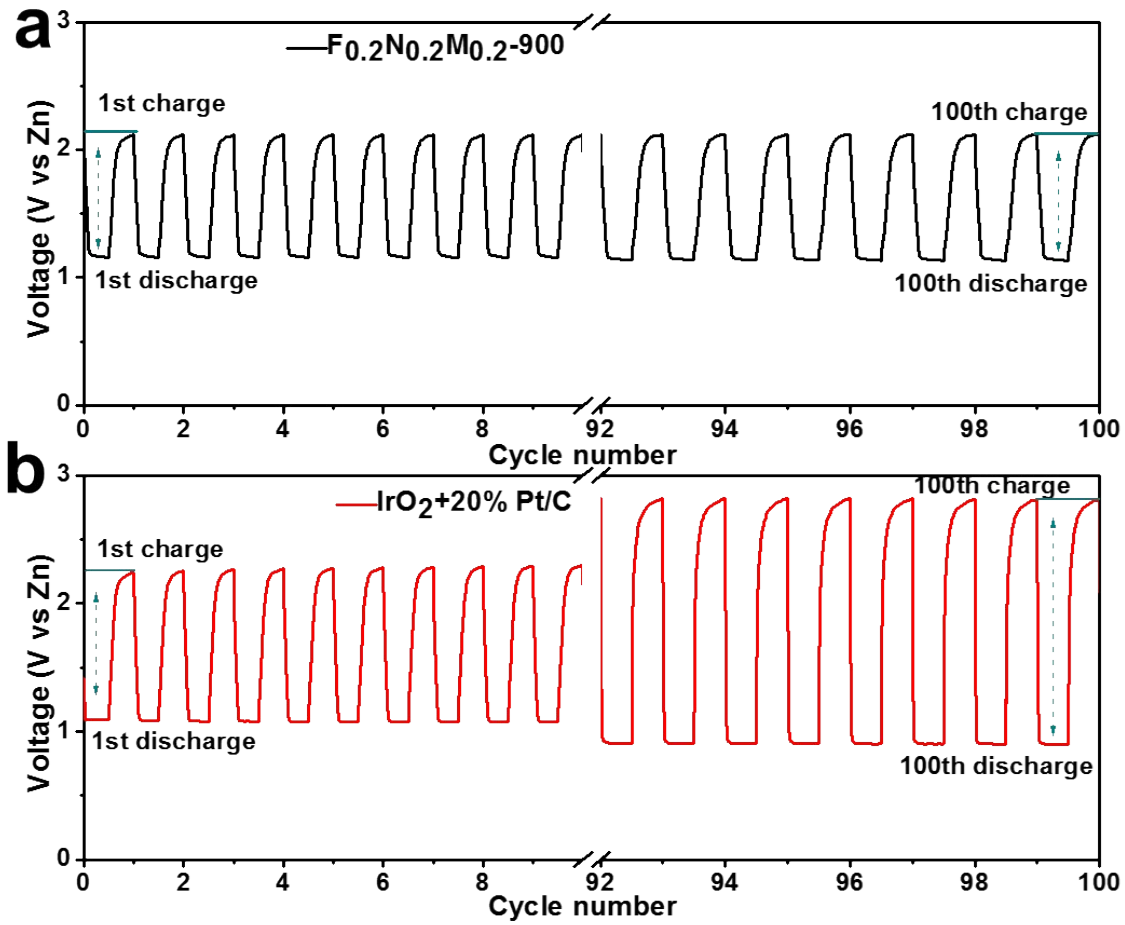

Fig. S26 Cycling performances of the rechargeable Zn-air battery with the (a) $F_{0.2}N_{0.2}M_{0.2}$-900 and (b) commercial IrO_2+20% Pt/C catalysts as the air electrodes at 10 mA cm^{-2} with a duration of 20 min per cycle.

Table S1 Comparisons of the ORR and OER performances for $F_{0.2}N_{0.2}M_{0.2}$-900 with other non-precious metal carbon electrocatalysts in 0.10 M KOH.

Catalysts	ORR		OER	References
	E^b_{onset}/V	$E^b_{1/2}$/V	η^a at 10 mA/cm^2 (mV)	
Fe-derived NCNT	0.89	0.71		2
pPMF	0.973	0.879		3
G/CNT/Co	0.95	0.86		4
BCN-FNHs	-	0.861		5
Co@N-CNTs-m	0.929	0.849		6
Co-C@NWCs	0.939	0.83		7
Co@Co_3O_4@PPD	~0.864	~0.794		8
HDPC	0.95	0.79		9
FeNi@NC			280	10
Co_4N/CNW/CC		0.8	310	11
NiO/CoN PINWs	0.89	0.68	300	12
CoO/hi-Mn_3O_4		~0.82	378	13
NiFeO@MnO_x	0.94	0.809	~470	14
Co_3O_4-HS			405	15
$Fe_xCo_{(1-x)}$-N/PC		0.812	405	16
Co-MOF@CNTs (5 wt%)	0.91	0.82	340	17
CoO@N/S-CNF	0.84	0.722	320	18
Co–N–C		0.8	310	19
Co/NC		0.83	460	20
Co_3O_4/NRGO	0.92	0.83	420	21
$F_{0.2}N_{0.2}M_{0.2}$-900	0.970	0.873	416	This work

E^b: potential in basic solution
pPMF: porous bamboo-like carbon nanotube/Fe_3C nanoparticles
BCN-FNHs: bamboo-like carbon nanotube (b-CNT)/Fe_3C nanoparticle (NP) hybrids
Co@N-CNTs-m: Co nanoparticle-encapsulated N-doped carbon nanotube
HDPC: heteroatom (N, P, Fe) ternary-doped, porous carbons
Co_4N/CNW/CC: composite containing Co_4N, carbon fibers network, and carbon cloth
NiO/CoN PINWs: NiO/CoN porous interface nanowires arrays
hi-Mn_3O_4: high-index facet Mn_3O_4nano-octahedrons
FeNi@NC: single layer graphene encapsulating FeNi
Co_3O_4-HS: Co_3O_4 hollow spheres
CoO@N/S-CNF: CoO nanoparticles into nitrogen and sulfur co-doped carbon nanofiber networks
Co_3O_4/NRGO: Co_3O_4/N-doped reduced graphene oxide

References

1. Y. Han, J. Zhai, L. Zhang and S. Dong, *Nanoscale*, 2016, 8, 1033-1039.
2. G.-L. Tian, Q. Zhang, B. Zhang, Y.-G. Jin, J.-Q. Huang, D. S. Su and F. Wei, *Adv. Fun. Mater.* 2014, 24, 5956-5961.
3. W. Yang, X. Yue, X. Liu, L. Chen, J. Jia, S. Guo, *Nanoscale,* 2015, 8, 959-964.
4. V. Vij, J. N. Tiwari and K. S. Kim, *ACS Appl. Mater. Inter.*, 2016, 8, 16045-16052.
5. W. Yang, X. Liu, X. Yue, J. Jia and S. Guo, *J. Am. Chem. Soc.*, 2015, 137, 1436-1439.
6. S. L. Zhang, Y. Zhang, W. J. Jiang, X. Liu, S. L. Xu, R. J. Huo, F. Z. Zhang and J. S. Hu, *Carbon*, 2016, 107, 162-170.
7. Y. Li, F. Cheng, J. Zhang, Z. Chen, Q. Xu and S. Guo, *Small*, 2016, 12, 2839-2845.
8. Z. Wang, B. Li, X. Ge, F. W. Goh, X. Zhang, G. Du, D. Wuu, Z. Liu, T. S. Andy Hor, H. Zhang and Y. Zong, *Small*, 2016, 12, 2580-2587.
9. Z. Guo, Z. Xiao, G. Ren, G. Xiao, Y. Zhu, L. Dai and L. Jiang, *Nano Res.*, 2016, 9, 1244-1255.
10. J. Yang, F. Zhang, X. Wang, D. He, G. Wu, Q. Yang, X. Hong, Y. Wu and Y. Li, *Angew. Chem. In. Edit.*, 2016, 55, 12854-12858.
11. F. Meng, H. Zhong, D. Bao, J. Yan and X. Zhang, *J. Am. Chem. Soc.*, 2016, 138, 10226-10231.
12. J. Yin, Y. Li, F. Lv, Q. Fan, Y.-Q. Zhao, Q. Zhang, W. Wang, F. Cheng, P. Xi and S. Guo, *ACS Nano*, 2017, 11, 2275-2283.
13. C. Guo, Y. Zheng, J. Ran, F. Xie, M. Jaroniec and S.-Z. Qiao, *Angew. Chem. In. Edit.*, 2017, 56, 8539-8543.
14. Y. Cheng, S. Dou, J.-P. Veder, S. Wang, M. Saunders and S. P. Jiang, *ACS Appl. Mater. Inter.*, 2017, 9, 8121-8133.
15. Y. Chuan Tan and H. Chun Zeng, *Chem. Commun.*, 2016, 52, 11591-11594.
16. M. Li, T. T. Liu, L. Q. Fan, X. J. Bo and L. P. Guo,*J. Alloy. Compd.*, 2016, 686, 467-478.
17. Y. Fang, X. Li, F. Li, X. Lin, M. Tian, X. Long, X. An, Y. Fu, J. Jin and J. Ma, *J. Power Sources*, 2016, 326, 50-59.
18. T. Liu, Y. F. Guo, Y. M. Yan, F. Wang, C. Deng, D. Rooney and K. N. Sun, *Carbon*, 2016, 106, 84-92.
19. F. L. Meng, H. X. Zhong, D. Bao, J. M. Yan and X. B. Zhang, *J. Am. Chem. Soc.*, 2016, 138, 10226-10231.
20. A. Aijaz, J. Masa, C. Rosler, W. Xia, P. Weide, A. J. Botz, R. A. Fischer, W. Schuhmann and M. Muhler, *Angew. Chem. In. Edit.,* 2016, 55, 4087-4091.
21. K. Kumar, C. Canaff, J. Rousseau, S. Arrii-Clacens, T. W. Napporn, A. Habrioux and K. B. Kokoh, *J. Phys. Chem. C*, 2016, 120, 7949-7958.